THE ASTROPHYSICAL JOURNAL, 492:782–787, 1998 January 10

DETECTION OF ABSORPTION-LINE FEATURES IN THE X-RAY SPECTRA OF THE GALACTIC SUPERLUMINAL SOURCE GRO J1655−40

Y. UEDA,[1] H. INOUE,[1] Y. TANAKA,[1,2] K. EBISAWA,[3] F. NAGASE,[1] T. KOTANI,[4] AND N. GEHRELS[3]
Received 1997 May 13; accepted 1997 August 22

ABSTRACT

We report the detection of iron K-absorption lines in the energy spectra of the superluminal jet source GRO J1655−40. We observed the source with *ASCA* on four occasions from 1994 through 1996. Significant absorption-line features were found at 6.63 ± 0.07 keV when the X-ray intensity was low (0.27–0.57 crab) and at 6.95 ± 0.10 keV when the intensity was high (2.2 crab). The former are interpreted as resonance absorption lines from helium-like iron and the latter are those from hydrogen-like iron, respectively. This gives direct evidence for the presence of highly ionized plasma in a nonspherical configuration in the vicinity of the black hole. The change of the ionization state of iron suggests that the plasma is photoionized by X-ray irradiation. The observed equivalent width (about 60 eV for the helium-like Kα line) and the ionization parameter ξ ($\sim 10^3$) constrain the size of the plasma to $\sim 10^{10}$ cm. The similarity of these properties to those of the other superluminal source GRS 1915+105 may imply some connection between the presence of such highly ionized plasma and the formation of relativistic jets.

Subject headings: stars: individual (GRO J1655−40) — X-rays: stars

1. INTRODUCTION

The X-ray nova GRO J1655−40 (Nova Sco 1994) is one of the only two Galactic superluminal sources (the other is GRS 1915+105; Mirabel & Rodriguez 1994). It was discovered with BATSE onboard the *Compton Gamma Ray Observatory* (*CGRO*) on 1994 July 27 (Zhang et al. 1994; Harmon et al. 1995). Soon after the discovery, radio and optical identifications of GRO J1655−40 were performed (Campbell-Wilson & Hunstead 1994; Bailyn et al. 1995a). Following the X-ray outbursts, the radio image showed twin jets extending in the opposite directions with superluminal motions (Tingay et al. 1995). The analysis of radio images with a kinetic model suggests that the inclination angle of the jet is 85° (Hjellming & Rupen 1995). Optical observations have shown that the system is a binary and give a large mass function, indicating the compact object is a black hole (Bailyn et al. 1995b). From the optical observation carried out in 1996 March when GRO J1655−40 was in quiescence, the mass of the central object and the inclination of the system are derived to be $7.02 \pm 0.22\ M_\odot$ and $69\overset{\circ}{.}5 \pm 0\overset{\circ}{.}08$, respectively (Orosz & Bailyn 1997).

GRO J1655−40 is the only black hole binary system with dynamical mass evidence that exhibits superluminal jets. In this paper we report results of the *ASCA* observations of GRO J1655−40 on four occasions from 1994 to 1996. We focus on the characteristic spectral features observed in the iron K band (5–10 keV). The broadband spectral analysis of the observation in 1995 is reported in Zhang et al. (1997).

2. OBSERVATIONS

The *ASCA* satellite (Tanaka, Inoue, & Holt 1994), carrying four identical X-Ray Telescopes (XRT; Serlemitsos et al. 1995) coupled to the two Solid-State Imaging Spectrometers (SIS; Burke et al. 1994) and the two Gas Imaging Spectrometers (GIS; Ohashi et al. 1996), performed four observations of GRO J1655−40 in the 0.5–10 keV energy band on 1994 August 23 (epoch I), 1994 September 27–28 (epoch II), 1995 August 15–16 (epoch III), and 1996 March 23–25 (epoch IV). In Table 1, the observation log is shown together with the mean intensity. All the GIS data were taken in the PH normal mode and the SIS in either the Bright or the Faint mode. The X-ray intensity during epoch IV was very low (10^{-13} ergs cm^{-2} s^{-1} [2–10 keV]; in total, $\sim$300 source photons are detected with the SIS) and does not allow us to perform a detailed spectral analysis. According to the intensity, we hereafter refer to epochs I and II together as "the low state" and epoch III as "the high state." Note that this is not equivalent to the canonical definition of the low state (hard state) and the high state (soft state) for black hole candidates (e.g., Tanaka & Lewin 1995). The first two *ASCA* observations (epochs I and II) correspond to times when the source was weak in the BATSE hard X-ray band (20–100 keV); the first observation was between the first and second hard X-ray outbursts, and the second one was between the second and third outbursts (Harmon et al. 1995). On the other hand, epoch III corresponds to the middle of the hard X-ray outburst of 1995 August (Zhang et al. 1997).

Figure 1 shows the light curves of epochs I, II, and III obtained with the GIS in the 0.7–10 keV band together with the spectral hardness ratio between two energy bands, 0.7–4 keV and 4–10 keV. Dead-time correction was performed using the monitor counts (Makishima et al. 1996). Data when the satellite attitude was not stable just after maneuvers were excluded. A diplike intensity change was detected in epoch I. In epochs II and III, on the other hand, the intensity remained roughly constant. The origin of the dip in epoch I has not been fully understood. Recent *ASCA* observations during the outburst of 1997 February revealed that there is no X-ray eclipse over the full orbital period. This is consistent with the inclination of 70° determined from the optical observation. Therefore, the dip might be

[1] Institute of Space and Astronautical Science, 3-1-1, Yoshinodai, Sagamihara, Kanagawa 229, Japan.
[2] Astronomical Institute "Anton Pannekoek," University of Amsterdam, Kruislaan 403, 1098 SJ Amsterdam, The Netherlands.
[3] NASA/Goddard Space Flight Center, Greenbelt, MD 20771.
[4] Institute of Physical and Chemical Research (RIKEN), 2-1 Hirosawa, Wako, Saitama 351-01, Japan.

TABLE 1

OBSERVATIONS OF GRO J1655−40 WITH *ASCA*

Epoch	State[a]	Start[b]	End[b]	SIS Mode	Exposure (s)[b]	Flux (2–10 keV)[c]
I.....	Low	1994 Aug 23 12:00	1994 Aug 23 13:50	Bright	2530	6.8
I.....	Dip	1994 Aug 23 14:57	1994 Aug 23 20:14	Bright	4450	1.7
I.....	Low	1994 Aug 23 20:56	1994 Aug 23 21:49	Bright	1550	4.5
II.....	Low	1994 Sep 27 14:00	1994 Sep 28 04:00	Faint[d]/Bright	16170/1910	12
III.....	High	1995 Aug 15 10:50	1995 Aug 16 04:20	Bright[d]	18750	47
IV.....	Off	1996 Mar 23 01:32	1996 Mar 25 19:17	Faint/Bright	84080 (total)	2×10^{-4}

[a] Refer to § 2 for definitions.
[b] Based on the data selection for the SIS.
[c] Mean intensity in units of 10^{-9} ergs cm^{-2} s^{-1} (2–10 keV).
[d] The SIS data suffered telemetry saturation.

due to occultation by the accretion disk or due to an intrinsic change of the X-ray–emitting region. Note that the intensity dip does not accompany spectral hardening and, hence, cannot be accounted for by absorption by cold matter. This is different from the absorption dips commonly observed from other X-ray binaries such as Cyg X-1 (e.g., Ebisawa et al. 1996) that accompany clear spectral hardening.

3. ANALYSIS AND RESULTS

We found the energy spectra during epochs I and II to be similar to each other, except during the dip. Hence, we combined data from epochs I and II excluding the dip and calculated average spectra for the three different intensity states: the dip, the low state (out of the dip), and the high state. We analyzed both the GIS and the SIS data after the standard data selection. We did not subtract the background, which is negligible compared with the high count rate from the source. A systematic error of 2% is included for each energy bin of the GIS spectra, due to the calibration uncertainty (Fukazawa, Ishida, & Ebisawa 1997).

In the analysis of the SIS data, we combined the Bright mode and the Faint mode data and summed up the spectra over SIS0 and SIS1 to improve statistics. The uncertainties of the energy scale and the energy resolution are estimated to be ∼1% and about a few tens of eV, respectively, considering the systematic error in the absolute gain scale and the intensity dependence of the charge transfer inefficiency (e.g., Dotani et al. 1997). GRO J1655−40 was so bright that the SIS raw spectra were contaminated with double photon (pileup) events. After excluding data in the core region within 2′.4 radius in the low state and 3′.2 in the high state, respectively, we further corrected for the remaining effect on the spectra by subtracting the pileup components by the method described in Ebisawa et al. (1996). We checked the accuracy of this calculation by performing a Monte Carlo simulation and found it to be accurate within 10% in the corrected spectra. Note that the spectral structures in the iron energy band we report below are much larger and are not affected by the systematic errors caused by this procedure.

3.1. *Continuum Model*

First, we fit the GIS spectra in the 1.2–10 keV range with a simple model. Figure 2 shows the raw GIS spectra for each intensity state. The whole spectra are roughly represented by a cutoff power-law model, $E^{-\Gamma} \exp(-E/E_{\rm fold})$, where Γ and $E_{\rm fold}$ are a photon index and a folding energy, respectively. The fit with a single-cutoff power-law model (with interstellar absorption) is, however, far from accept-

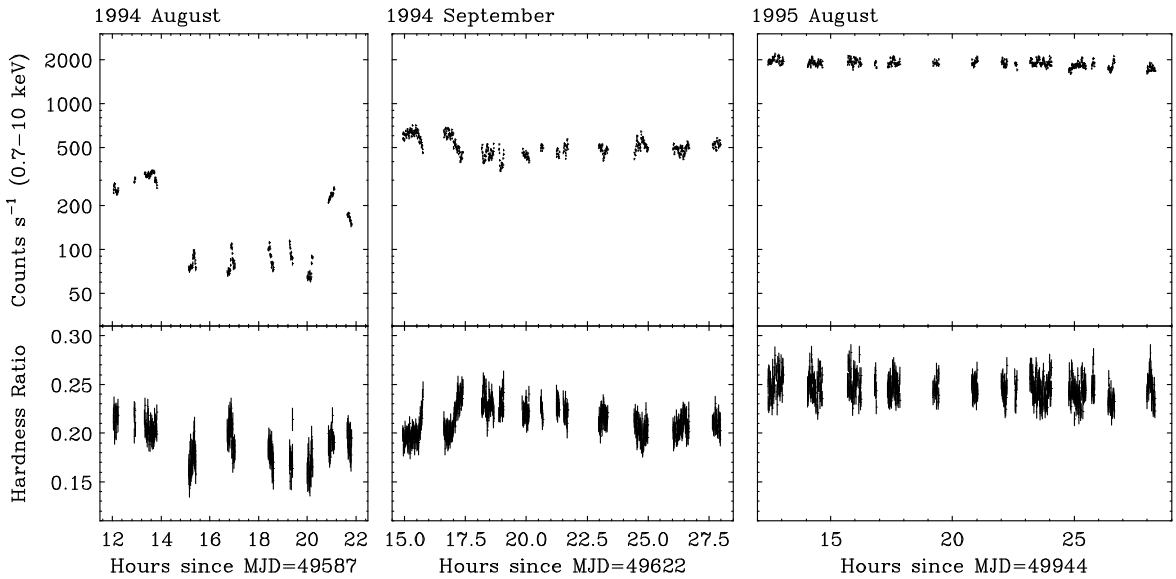

FIG. 1.—Light curves of GRO J1655−40 on 1994 August 23 (epoch I), 1994 September 27 (epoch II), and 1995 August 15 (epoch III) obtained with the *ASCA* GIS (GIS2 and GIS3 are summed). *Upper panel:* The count rate within a radius of 6 mm in the 0.7–10 keV band. *Lower panel:* Hardness ratio between two energy bands, 0.7–4 keV and 4–10 keV.

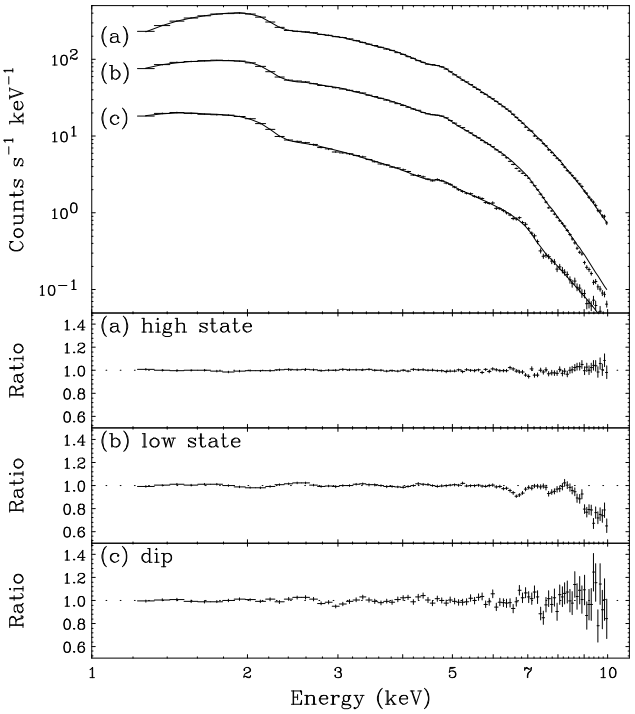

FIG. 2.—GIS folded spectra of GRO J1655−40 in the three distinct intensity states: (*a*) the high state, (*b*) the low state out of the dip, and (*c*) the dip. The solid line shows the continuum model based on the best-fit parameters given in Table 2, excluding the contribution of the local structures (see § 3.2). In the lower panel, the ratio of the data to the model is shown.

able, except for the high state ($\chi^2/\nu = 84/89$, 2900/89, and 573/89 for the high state, the low state, and the dip, respectively). This is because of complex structures in the iron K band, as discussed below. From Figure 2, it is noticed that the spectrum of the high state is slightly harder than that of the low state. The extrapolation of the spectra toward higher energies is consistent with the BATSE observations in both epochs (Harmon et al. 1995; Zhang et al. 1997). Note that the continuum shape could be also described approximately by the so-called multicolor disk model (MCD model; e.g., Mitsuda et al. 1984) plus a power-law component, a typical spectrum seen from black hole candidates in the soft state (e.g., Tanaka & Lewin 1995). The fitting result with this model for the high-state spectrum is given in Zhang et al. (1997).

An iron K-edge structure is suggested around 7.1 keV in the dip and the low-state spectra of Figure 2. This indicates the presence of absorption by cool matter, but little absorption is observed in the low-energy band. A reflection component may also reproduce the iron edge structure with a small amount of low-energy absorption, but it should be accompanied by a strong fluorescent line at 6.4 keV. However, the 90% upper limit of the line equivalent width with respect to the reflection component is only ~ 20 eV, as opposed to the predicted value of ~ 1 keV (e.g., Inoue 1985). Hence, a partial absorption (or partial covering) model, in which a part of the emission is heavily absorbed and the other part is not, is a likely explanation. In fact, it improves the fit to the GIS 1.2–10 keV spectra significantly in the low state and the dip ($\chi^2/\nu = 508/87$ and 118/87). Furthermore, in addition to the partial absorption, we found that inclusion of the smeared edge model (Ebisawa et al. 1994) at 7.1 keV gave a significantly better fit ($\chi^2/\nu = 305/86$ and 104/86 for the low state and the dip, respectively). The optical depth obtained for the low state is $\tau_s = 3.3 \pm 0.8$ with an edge energy and a width fixed at 7.11 keV and 10 keV, respectively. This means the edge structure at 7.1 keV is broader than a sharp edge contained in the the partial absorption model itself. The broad edge could be explained if the X-ray absorber in the line of sight consists of slightly ionized (warm) matter and nonionized (cold) matter, which is likely to be the case.

3.2. *Spectral Features in the Iron K Band*

To investigate the structures around the iron K band in more detail, we next examined the SIS spectra, which have superior energy resolution. Figure 3 shows the SIS spectra (*a*) in the high state, (*b*) in the low state outside the dip, and (*c*) in the dip. In the lower panel, we present the data in the form of a ratio to a single-cutoff power-law model to emphasize all local structures. Characteristic spectral structures are clearly seen near 7 keV and are quite different in the three states. In the dip and the low state, the edge struc-

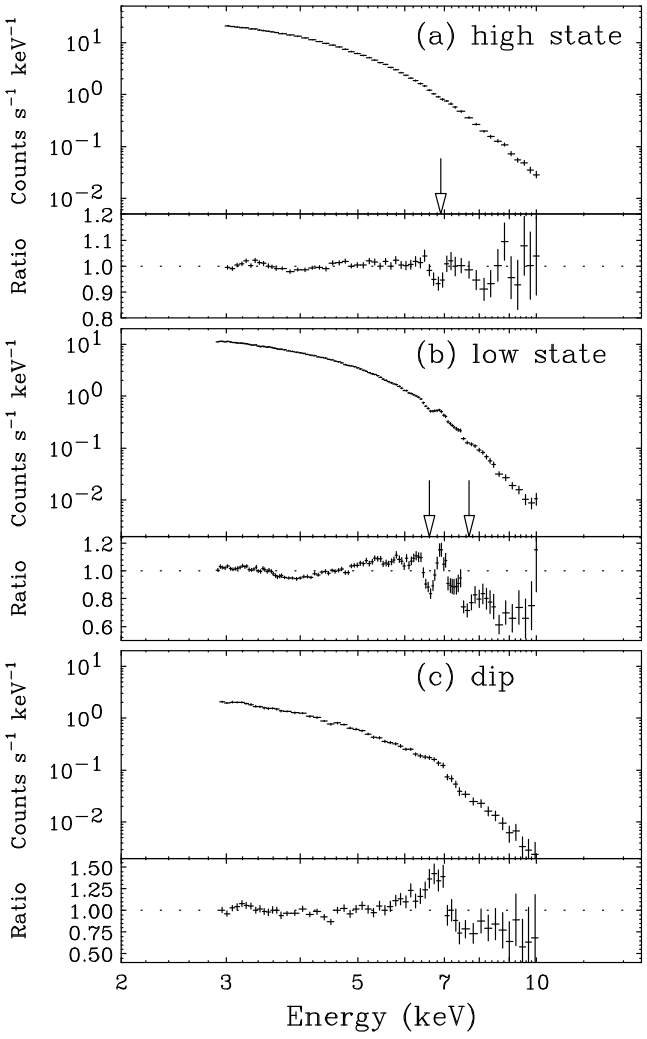

FIG. 3.—SIS raw spectra above 3 keV in (*a*) the high state, (*b*) the low state out of the dip, and (*c*) the dip. The lower panel shows the ratio of the data to a single-cutoff power-law model. In the low state, absorption lines are clearly detected at ~ 6.6 keV (and possibly at ~ 7.7 keV). In the high state, an absorption-line feature is found at ~ 7.0 keV. These absorption lines are denoted by arrows in the figure. A clear edge structure is seen at 7.1 keV in both the dip and the low-state spectrum.

ture at 7.1 keV found in the GIS data is confirmed. We hereafter limit the energy range to 5–10 keV in the spectral analysis, because the SIS data are not suitable to determine a continuum over a wide energy range because of uncertainties of the effective area under the telemetry saturation.

The spectral feature at the iron K band in the low state (out of the dip) is very intriguing. Clearly, we find an absorption-line feature around 6.6 keV together with the iron K edge at 7.1 keV. *F*-tests verify the significance of the absorption line. The *F*-value, $(\Delta\chi^2/\nu_1)/(\chi^2/\nu_2)$, is 30.8 for dof $(\nu_1, \nu_2) = (3, 53)$ when we add an absorption line, modeled by a negative Gaussian, to the same continuum model as used for the GIS data that contains the edge structure at 7.1 keV. Therefore, the absorption-line feature is significant at the greater than 99% confidence level. In addition, an absorption line around 7.7 keV is marginally seen, although it is not statistically significant [the *F*-value is 2.1 for $(\nu_1, \nu_2) = (2, 51)$]. On the other hand, in the spectrum of the high state, an absorption-line feature is found at 6.95 ± 0.10 keV with no significant edge structure. An *F*-test for this spectrum also verifies the significance of the absorption line at 99% confidence level [$F = 7.24$ for $(\nu_1, \nu_2) = (3, 27)$].

To check the consistency with the GIS data, we again fit the GIS spectra in the 1.2–10 keV band, adding the absorption lines to the continuum model, except for the dip spectrum, where no significant absorption line was detected. In the low state, besides the two absorption lines at 6.6 and 7.7 keV, we detected a significant edge structure at 8.8 keV in the GIS spectrum. The edge energy and the optical depth is 8.81 ± 0.12 and 0.38 ± 0.07 keV, respectively, when a simple edge model is applied. Although the feature is not significant in the SIS spectrum due to the poor statistics above 8 keV, we confirmed that the GIS result is consistent with the SIS data. By including these local features to the continuum model (i.e., a partial covering cutoff power-law model with the smeared edge), the whole GIS spectra were successfully fit in the 1.2–10 keV band. The results of the spectral fit are summarized in Table 2. For the high-state spectrum, we used a single-cutoff power-law model with interstellar absorption as a continuum because neither the partial absorption nor the smeared edge is necessary. The parameters of the absorption lines are determined by the SIS data in the 5–10 keV band. We verified their parameters obtained with the GIS are fully consistent with the SIS results. In Figure 2, we superpose the best-fit continuum model on the data with a solid line and show the ratio of the data to the model in the lower panel. In this plot, to emphasize the local spectral features, we excluded the contributions of the absorption lines (for the high and the low state) and the edge at 8.8 keV (for the low state) from the best-fit model.

4. DISCUSSION

We have detected iron K-absorption lines from the energy spectra of GRO J1655−40. This is the first clear detection of the iron absorption lines from accretion powered compact X-ray sources. The energies of the two absorption lines found in the low state (6.63 ± 0.07 and 7.66 ± 0.13 keV) are consistent with those of Kα and Kβ lines from He-like iron ions, taking account of a 1% systematic error in the energy scale. Furthermore, an edgelike structure is seen at 8.81 ± 0.12 keV in the GIS spectrum in the low state. The edge energy is consistent with the K edge of He-like iron. On the other hand, the energy of the

TABLE 2

SPECTRAL FITS IN THE 1.2–10 keV BAND

Parameters	High State	Low State	Dip
Reduced χ^2 (dof)[a]	0.77 (87)	1.24 (81)	1.21 (86)
Continuum Model[b]			
f	0 (fixed)	0.35 ± 0.06	0.65 ± 0.06
N_{H1} (10^{22} cm^{-2})	...	36 ± 5	62 ± 9
Γ	0.39 ± 0.05	-0.34 ± 0.14	0.79 ± 0.25
E_{fold} (keV)	2.00 ± 0.04	1.48 ± 0.10	$2.42^{+0.54}_{-0.37}$
A (cm^{-2} s^{-1} keV^{-1})	19.8 ± 0.6	4.5 ± 0.4	2.00 ± 0.27
N_{H2} (10^{22} cm^{-2})	0.74 ± 0.03	<0.08	<0.14
τ_s	...	3.3 ± 0.8	2.7 ± 1.4
Spectral Features in the Iron K Band[c]			
Absorption-line energy (keV)[d]	6.95 ± 0.10	$6.63 \pm 0.07/7.66 \pm 0.13$	...
1 σ line width (eV)	<150	$<75/<130$	...
Equivalent width (eV)	25^{+13}_{-11}	$61^{+15}_{-13}/35^{+30}_{-29}$	...
Identification	Fe XXVI Kα	Fe XXV Kα/Fe XXV Kβ	...
Edge energy (keV)	...	8.81 ± 0.12	...
Optical depth	...	0.38 ± 0.07	...

NOTE.—Errors are 90% confidence limits for a single parameter.

[a] A value obtained for the GIS 1.2–10 keV data when the spectral features in the iron K band are included in the model.

[b] The model is $[fe^{-N_{H1}\sigma(E)} + (1-f)]e^{-N_{H2}\sigma(E)}(AE^{-\Gamma}e^{-E/E_{fold}})S(E)$, where E is the photon energy in keV, $\sigma(E)$ is the photoelectric absorption cross section (Morisson & McCammon 1983), f is the covering fraction, N_{H1} is the column density of the local absorber, N_{H2} is the column density of the interstellar absorption, Γ is the photon index, E_{fold} is the folding energy, and A is the normalization. $S(E)$ represents the smeared edge model (Ebisawa et al. 1994): $S(E) = 1$ for $E < E_s$, and $S(E) = \exp(-\tau_s(E/E_s)^{-2.67}[1 - e^{(E_s-E)/\sigma_s}])$ for $E > E_s$, where E_s and σ_s are fixed at 7.11 keV and 10 keV, respectively. The GIS data in 1.2–10 keV are used. See § 3.1 for details.

[c] Parameters of absorption lines are determined by the SIS data, and that of edge is by the GIS data. See § 3.2 for details.

[d] Error includes the systematic error (1%) and the statistical error.

absorption line during the high state was 6.95 ± 0.10 keV, which is consistent with that of Kα line from H-like iron ions. These absorption lines of He-like or H-like iron are probably attributable to resonant absorption in a highly ionized plasma located in the line of sight. In such a hot plasma, as iron is ionized to He-like ions, other lighter elements will be almost fully ionized. This is consistent with absence of large absorption in the spectrum in the low-energy band.

A resonance absorption of an X-ray photon by an iron ion should be followed by reemission of a photon with the same energy. Hence, the absorption would not be detected if the incident X-ray emission and the ambient hot plasma are both isotropic and the plasma is at rest. If the plasma isotropically flows inward or outward, we should have detected an emission line at the rest-frame energy (6.7 keV for Fe XXV) accompanied by redshifted or blueshifted absorption lines, like a P Cygni profile. This is not the case, suggesting an anisotropy in the X-ray emission and/or the distribution of matter. The relativistic jets observed in the radio band are a strong evidence of anisotropy near the central engine. However, the jet itself cannot be the line absorber, since, if so, a redshift by several tens percent (which is calculated from the jet parameters; Hjellming & Rupen 1995), should have been observed in the absorption-line energies, whereas the measured energy shift is less than 1%.

The parameters of the absorption lines contain valuable information on the physical condition of the line-absorbing matter. The center energy directly reflects the ionization state of the hot plasma, while the equivalent width is closely related to the column density of the plasma. Figure 4 shows the so-called curve of growth for the Kα absorption line from He-like iron, where an expected equivalent width is plotted as a function of a column density of the iron ions for several plasma temperatures (0.1, 1, and 10 keV). Note that a temperature of 10 keV is too high to keep the ionization state of irons in the He-like stage and, hence, should be taken as an upper limit. Here we assume that the absorbing matter exists only in the direction of the line of sight around the X-ray emitter. Transition of $^1S_0 \rightarrow {}^1P_1$ (resonance line) and $^1S_0 \rightarrow {}^3P_1$ (intercombination line) are considered, since other transitions are negligible. The transition probability and the line energy are taken from Mori, Otsuka, & Kato (1979, and references therein). As seen from the figure, the observed equivalent width, 61^{+15}_{-13} eV, indicates that the iron column density of the plasma is 4×10^{17}–4×10^{18} cm^{-2}, which corresponds to a hydrogen column density of 2×10^{22}–2×10^{23} cm^{-2}, assuming cosmic elemental abundance and iron ions in the He-like stage. Considering the more realistic case that the absorbing matter also exists in other directions, the column density derived above gives only a lower limit because the absorption line is compensated by the reemission from the surrounding matter. On the other hand, the line absorber should be optically thin to Thomson scattering, $N_{\rm H} < 10^{24}$ cm^{-2}, or the narrow absorption line would not have been observed. We finally obtain the hydrogen column density of the line-absorbing plasma as 2×10^{22} cm$^{-2} < N_{\rm H} < 10^{24}$ cm^{-2}. Note that the observed optical depth of the K edge of the He-like iron at 8.8 keV, $\tau \simeq 0.4$, corresponds to $N_{\rm H} \simeq 3 \times 10^{23}$ cm^{-2}, assuming the cosmic abundance. This is consistent with the result derived from the absorption line.

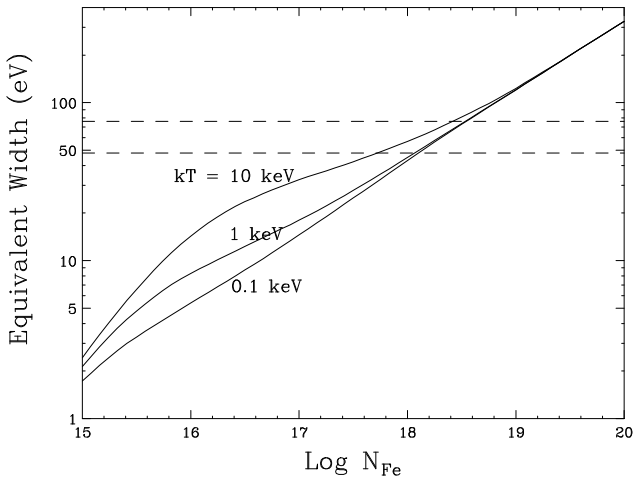

FIG. 4.—Curve of growth for the Kα absorption line from He-like iron, where the equivalent width is calculated as a function of the column density of He-like iron (refer to § 4 for details). Three electron temperatures ($kT = 0.1$, 1, and 10 keV) are assumed for the plasma in the line of sight. The two dashed lines represent the 90% statistical error for the equivalent width observed in the low state.

We have discovered that the ionization of iron changed from He-like to H-like as the X-ray luminosity increased from the low state to the high state. This suggests that the plasma is photoionized by the X-ray irradiation. For iron in the line absorber to be ionized to the He-like stage, the ionization parameter, $\xi \equiv L/nr^2$, where L is the X-ray luminosity, n is the electron number density, and r is the distance from the X-ray source, should be $\sim 10^3$ ergs cm s^{-1}, assuming X-ray heating is dominant (see, e.g., Kallman & McCray 1982). In the observations during the low state, the X-ray luminosity above ~ 9 keV (which is responsible for the photoionization of He-like iron) is about 10^{36} ergs s^{-1} in the definition by Kallman & McCray (1982) at a likely distance of 3 kpc (Tingay et al. 1995; Bailyn et al. 1995a; Greiner, Predehl, & Pohl 1995). Hence, nr^2 is $\sim 10^{33}$ atoms cm^{-1} using $\xi \sim 10^3$. From the previous discussion, the hydrogen column density of the plasma is $nr \sim 10^{23}$ cm^{-2}. Combining the two conditions, the distance (or size) of the line absorber from the central X-ray source is derived to be $\sim 10^{10}$ cm. A plasma at $\sim 10^{10}$ cm from the center having an anisotropic structure is a likely candidate for the line absorber. A possible picture of the system is that we are viewing the central X-ray emission through a slablike accretion disk corona extending above the disk plane with an inclination angle of 70°.

Note that similar absorption features have also been detected from the other superluminal jet source, GRS 1915+105 (Ebisawa 1996). This might suggest a connection between the presence of the relativistic jets and the presence of highly ionized plasma with nonspherical configuration responsible for the absorption lines. Alternatively, the absorption-line feature may not be related to the jets, but may be merely a consequence of the large inclination angles of the systems (the inclination angle of GRS 1915+105 is estimated as 70°; Mirabel & Rodriguez 1994). In this context, further searches for absorption-line features in both jet sources and nonjet sources are important.

We thank A. C. Fabian, W. N. Brandt, and S. N. Zhang for useful discussions. We appreciate valuable comments from K. Masai, J. Ichimura, M. Ishida, and T. Kii on the atomic physics.

REFERENCES

Bailyn, C. D., et al. 1995a, Nature, 374, 701
Bailyn, C. D., Orosz, J. A., McClintock, J. E., & Remillard, R. A. 1995b, Nature, 378, 157
Burke, B. E., Mountain, R. W., Daniels, P. J., Cooper, M. J., & Dolat, V. S. 1994, IEEE Trans. Nucl. Sci., 41, 375
Campbell-Wilson, D., & Hunstead, R. 1994, IAU Circ., Nos. 6052, 6055
Dotani, T., et al. 1997, *ASCA* News, No. 4, 14
Ebisawa, K. 1996, in X-Ray Imaging and Spectroscopy of Cosmic Hot Plasmas, ed. F. Makino & K. Mitsuda (Tokyo: Universal Academy), 427
Ebisawa, K., Ogawa, M., Aoki, T., et al. 1994, PASJ, 46, 375
Ebisawa, K., Ueda, Y., Inoue, H., Tanaka, Y., & White N. E. 1996, ApJ, 467, 419
Fukazawa, Y., Ishida, M., & Ebisawa, K. 1997, *ASCA* News, No. 4, 3
Greiner, J., Predehl, P., & Pohl, M. 1995, A&A, 297, L67
Harmon, B. A., et al. 1995, Nature, 374, 703
Hjellming, R. M., & Rupen, M. P. 1995, Nature, 375, 464
Inoue, H. 1985, Space Sci. Rev., 40, 317
Kallman, T. R., & McCray, R. 1982, ApJS, 50, 263
Makishima, K., et al. 1996, PASJ, 48, 171
Mirabel, I. F., & Rodriguez, L. F. 1994, Nature, 371, 46
Mitsuda, K., et al. 1984, PASJ, 36, 741
Mori, K., Otsuka, M., & Kato, T. 1979, At. Data Nucl. Data Tables, 23, 195
Morrison, R., & McCammon, D. 1983, ApJ, 270, 119
Ohashi, T., et al. 1996, PASJ, 48, 157
Orosz, J. A., & Bailyn, C. D. 1997, ApJ, 477, 876
Serlemitsos, P. J., et al. 1995, PASJ, 47, 105
Tanaka, Y., Inoue, H., & Holt, S. S. 1994, PASJ, 46, L37
Tanaka, Y., & Lewin, W. H. G. 1995, in X-Ray Binaries, ed. W. H. G. Lewin, J. van Paradijs, & W. P. J. van den Heuvel (Cambridge Univ. Press), 126
Tingay, S. J., et al. 1995, Nature, 374, 141
Zhang, S. N., et al. 1994, IAU Circ., No. 6046
———. 1997, ApJ, 479, 381